nature communications



Article

https://doi.org/10.1038/s41467-024-52273-x

Optical tweezing of microparticles and cells using silicon-photonics-based optical phased arrays

Received: 2 May 2023

Accepted: 29 August 2024

Published online: 03 October 2024



Check for updates

Tal Sneh 1, Sabrina Corsetti 1, Milica Notaros, Kruthika Kikkeri, Joel Voldman¹ & Jelena Notaros **©**¹ ⋈

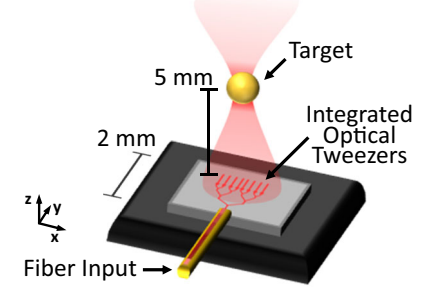
Integrated optical tweezers have the potential to enable highly-compact, lowcost, mass-manufactured, and broadly-accessible optical manipulation when compared to standard bulk-optical tweezers. However, integrated demonstrations to date have been fundamentally limited to micron-scale standoff distances and, often, passive trapping functionality, making them incompatible with many existing applications and significantly limiting their utility, especially for biological studies. In this work, we demonstrate optical trapping and tweezing using an integrated OPA for the first time, increasing the standoff distance of integrated optical tweezers by over two orders of magnitude compared to prior demonstrations. First, we demonstrate trapping of polystyrene microspheres 5 mm above the surface of the chip and calibrate the trap force. Next, we show tweezing of polystyrene microspheres in one dimension by non-mechanically steering the trap by varying the input laser wavelength. Finally, we use the OPA tweezers to demonstrate, to the best of our knowledge, the first cell experiments using single-beam integrated optical tweezers, showing controlled deformation of mouse lymphoblast cells. This work introduces a new modality for integrated optical tweezers, significantly expanding their utility and compatibility with existing applications, especially for biological experiments.

Optical traps and tweezers enable trapping and manipulation of particles through non-contact forces caused by optical intensity gradients and photon momentum transfer¹. Due to these properties, optical trapping has become a key technology for biological experimentation since it enables precise control over the position of and applied force on objects at the micron and submicron scale. For example, this technique has enabled insight into the biomechanics of DNA and motor proteins, helped classify and characterize cells, and yielded important data on the underlying biology of disease mechanisms¹⁻⁷. However, since standard optical tweezers consist of benchtop systems comprised of bulk-optical components, their cost, complexity, and need for specialized laboratory equipment have limited broad access to these standard bulk-optical tweezers.

Integrated-photonics-based optical tweezers offer exciting potential to resolve these challenges. Specifically, integratedphotonics-based tweezers can be mass manufactured in a compact form factor and at a much lower cost and can be densely integrated to increase trapping throughput. To date, integrated optical trapping has been demonstrated using evanescent fields from planar waveguides, optical resonators, and plasmonic devices⁸⁻¹⁶. While these systems offer significant advantages in form factor and complexity compared to standard bulk-optical systems, they have been restricted to trapping either directly on or within several microns from the surface of the chip (Fig. 1b). This significantly limits their widespread applicability in biophysics and cell experimentation, which typically involve sterile glass coverslips or cell culture wells that are at least 150-µm thick, since their

¹Research Laboratory of Electronics, Massachusetts Institute of Technology, Cambridge, MA 02139, USA. ⊠e-mail: notaros@mit.edu

(a) Integrated OPA Tweezers Concept



(b) Integrated Optical Tweezers Comparison

Tweezers System	Operating Distance	Active Tweezing
Plasmonic [13]	<1 μm	×
Waveguide [14]	<1 μm	×
Resonator [11]	<1 μm	✓
Microlens [12]	20 μm	×
OPAs (This Work)	5000 μm	>

Fig. 1 | **Integrated OPA tweezers concept. a** Conceptual diagram (not to scale) of the integrated OPA-based tweezers system showing a photonic chip emitting a focused beam and trapping a microsphere target. **b** Comparison of key considerations for previously demonstrated integrated optical tweezers versus the proposed integrated OPA-based tweezers system.

focal heights are too short to penetrate into these standard sample chambers. Without the ability to use these ubiquitous methods of sample preparation, these prior integrated optical tweezers could only be used in a narrow set of experiments, such as with back-end-of-theline microfluidics fabricated on top of the chips, which require additional time to fabricate, often necessitate disposal of the chip after each experiment due to contamination, and are non-sterile surfaces that are not compatible with the majority of biophysics, and especially cell, research. As such, extending standoff distances to the millimeter scale to enable compatibility with these standard sample-preparation methods is an important requirement for integrated optical tweezers to become a practical technology (and could even enable demonstrations in emerging in-vivo tweezing applications that require millimeter-scale standoff distances⁷). In addition, many of these prior integrated optical tweezers have been fundamentally limited to passive trapping demonstrations that lack active spatial tuning of the optical fields, which is necessary for both initial trapping of the target object and for optical tweezing or manipulation of the object (Fig. 1b)¹²⁻¹⁵. Together, these challenges have limited the implementation of these integrated optical tweezers for biophysics and cell experimentation.

In contrast, integrated optical phased arrays (OPAs), which enable emission and non-mechanical control of arbitrary free-space radiation patterns from compact silicon-photonics chips by applying relative phase delays to a series of on-chip antennas¹⁷⁻²³, have the potential to resolve these limitations of current integrated optical tweezers. Specifically, they provide a promising approach to extending the standoff operating distance by orders of magnitude (resolving the fundamental limitation on operating distance imposed by using evanescent-field trapping modalities), enabling active spatial tuning for tweezing functionality, and expanding to holographic multi-beam capability for high-throughput sorting in the future (Fig. 1b). However, motivated by applications such as LiDAR sensing and free-space optical communications, the majority of integrated OPA demonstrations to date have been limited to generating and steering beams in the far field by applying linear phase gradients¹⁷⁻²², which do not generate the tightlyfocused beam profiles required for optical trapping. Recently, our group proposed and demonstrated the first integrated OPAs that enable focusing beam profiles²³.

In this work, we demonstrate optical trapping and tweezing using an integrated OPA for the first time. The OPA system focuses the emitted light at a specific point in the radiative near field of the chip and provides a steerable potential-energy well in the plane of the sample that can be used to trap and tweeze microscale particles (Fig. 2a). By enabling this OPA approach, we are able to increase the standoff distance of integrated optical tweezers by over two orders of magnitude compared to prior demonstrations and show trapping and non-mechanical tweezing of polystyrene microspheres at a distance of 5 mm above the surface of a silicon-photonics chip. We then use the OPA tweezers to stretch mouse lymphoblast cells, showing, to the best of our knowledge, the first cell experiments using single-beam integrated optical tweezers. Overall, this work introduces a new modality for integrated optical tweezers, significantly expanding the utility and compatibility of integrated tweezers with both common biological experiments and emerging in-vivo trapping research by extending their focal heights to the millimeter scale, with promising applications ranging from DNA and protein experiments to cell manipulation and sorting.

Focusing integrated OPA system

In general, an integrated optical phased array (OPA) is a system comprised of an array of antennas that are fed with controlled phase and amplitude inputs into each antenna to emit arbitrary radiation patterns off of the chip. If the antennas are fed with a uniform amplitude and a linear phase distribution, the array is limited to generating and nonmechanically steering a diffracting beam in the far field of the array (as has been shown in the majority of OPA demonstrations to date)^{17–22}. An example simulated radiation pattern resulting from this traditional approach can be seen in Fig. 2a. In contrast, if a hyperbolic phase distribution, similar to the curvature of a lens, is applied across the antennas, the resulting radiation pattern will be tightly focused at a point in the radiative near field above the array (Fig. 2b)²³. This hyperbolic phase can be encoded modulo 2π , similar to a Fresnel lens. leading to the phase distribution shown in Fig. 2d. This novel focusing OPA modality and the resulting focused beam enable the light intensity gradients required to perform optical trapping.

To demonstrate this functionality, we designed and fabricated a splitter-tree-based focusing OPA system 23 . The system was fabricated in a CMOS-compatible foundry process at the State University of New York Polytechnic Institute's (SUNY Poly) Albany NanoTech Complex on a 300-mm silicon-on-insulator wafer with a buried oxide thickness of $2\,\mu m$. The silicon device layer is 220-nm thick and was patterned with 193-nm immersion lithography.

The system is designed to operate at a center wavelength of 1550 nm. At the system input, an inverse-taper edge coupler couples light into an on-chip silicon waveguide from an off-chip laser. A 9-stage splitter tree network comprised of compact Y-junction splitters²⁴ then evenly distributes the input power to 512 grating-based antennas with an antenna pitch of 2 µm. To apply the desired phase distribution for focusing in the array dimension (x), a phase bump device is placed before each antenna to impart a static phase delay dependent on the maximum width of the bump; the width of each bump is chosen such that the correct phase profile for focusing 5 mm above the chip is applied. Since the antennas are spaced with an antenna pitch larger than $\lambda/2$, the system also generates higher-order grating lobes in the array dimension; however, these lobes appear at larger angles and are far out of both the field of view and focal plane of experimentation, and, consequently, their main impact on the system is only reducing efficiency by drawing power from the main lobe. To enable focusing also in the antenna dimension (y), the period of the grating-based antennas is adiabatically chirped along the length of the antennas, varying the angle of emission such that the light from each

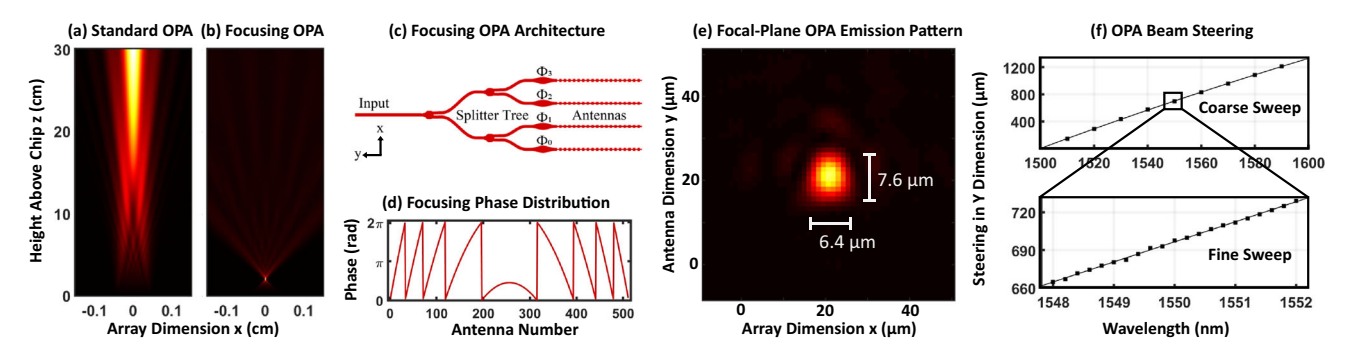


Fig. 2 | **Design and characterization of the focusing integrated OPA system.** Simulated array-factor intensity above the chip for **(a)** a standard non-focusing OPA and **(b)** a near-field-focusing OPA with a 20-mm focal height. **c** Schematic of a passive splitter-tree-based focusing OPA architecture with 4 antennas (not to scale). **d** Element phase distribution for a focusing OPA with a 20-mm focal height, 512

antennas, $2 \cdot \mu m$ antenna pitch, and 1550-nm wavelength. **e** Measured radiation pattern at the focal plane of the OPA, showing a tightly focused spot. **f** Experimental results showing coarse non-mechanical beam steering of the OPA spot in the antenna dimension, γ , versus input wavelength, with inset showing fine tuning.

perturbation along the antenna intersects at the focal height. Note that errors in the encoded phase due to fabrication variations will present themselves primarily as a degradation in the resulting spot quality and expansion of the beam waist. More details on the OPA design and fabrication can be found in²³.

The dimensions of the resulting focal spot, which impact the trapping efficiency, scale inversely with the OPA aperture size and linearly with the OPA focal height²³, allowing the characteristics of the system to be adjusted to fit the desired application. In this demonstration, we target polystyrene beads and cells with sizes around $10\,\mu\text{m}$. As a result, an aperture size of $1\,\text{mm}^2$ and focal height of 5 mm were chosen to provide a reasonable tradeoff between trapping efficiency, focal height, and system footprint.

Note that, for the aperture size and focal height chosen for this demonstration, the resulting focal spot size in the vertical dimension (z) is large, and the trap provides little confinement along the vertical axis. For many optical-trapping experiments, the lateral (x and y) trapping efficiency is more important than the vertical. However, some potential applications also require tight confinement in the vertical dimension. In these cases, a larger aperture size or shorter focal height could be chosen to provide micrometer-scale spot sizes in the vertical dimension, as well as the lateral dimensions²³.

To characterize the fabricated system, we utilize an Agilent 81600B tunable benchtop laser source and an optical system to image the focal plane of the OPA onto an InGaAs infrared (IR) camera (see Methods for details). The resulting radiation pattern in the focal plane of the OPA is shown in Fig. 2e. The fabricated system focuses tightly at the designed focal height of 5 mm, with a power full-width half-maximum (FWHM) of approximately $6.4 \mu m$ along the array dimension (x) and 7.6 µm along the antenna dimension (y), closely matching the expected FWHM of $6.6 \,\mu\text{m} \times 7.6 \,\mu\text{m}$ from simulation²³. We measure an optical fiber to main lobe (i.e. trap focal spot) efficiency of approximately -14.5 dB, with primary sources of loss attributed to edgecoupling loss, waveguide propagation loss, Y-junction splitter losses, and antenna emission losses, including power radiated to the grating lobes. These experimental results confirm that this focusing OPA system satisfies the requirements for static optical trapping of polystyrene particles and cells.

In order to enable the system to transform from a static optical trap to dynamic optical tweezers, the ability to precisely steer the position of the emitted focal spot is necessary. To enable steering of the focal spot in one dimension using the OPA system, we vary the input wavelength, which changes the effective period of the radiating antennas and, as a result, their angle of emission²³. As shown in Fig. 2f, the focal spot can be non-mechanically steered in the antenna dimension (i.e. in the *y* dimension) over a range larger than a millimeter

-useful for positioning the spot relative to the target object when optical trapping, as well as finely steered with micron-scale accuracy for precision force and position sensing. Since steering within the tens of microns region of interest for typical trapping experiments requires only small changes in emission angle and, therefore, input wavelength, the emitted power and, consequently, trap stiffness was experimentally found to remain consistent as the trap position is steered (note that, if steering over the entire millimeter range is necessary, the spot size will change²³ and, as a result, trap stiffness will begin to degrade). Since the spot steering mechanism is fundamentally based on the Bragg condition, in theory, the only limitation on the fidelity of steering is the wavelength step size and the stability of the laser input. Common scientific benchtop lasers, such as the Agilent systems used in this work, offer wavelength step sizes and stabilities in the range of a few picometers, corresponding to theoretical spot position variation in the tens of nanometers: this is significantly smaller than the position variation of a trapped particle due to random motion for the trap powers under study. Therefore, when used with most benchtop lasers, the strength of the trap and, as a result, the mean squared displacement of the trapped object will limit when two different trap locations will produce a meaningful displacement of the object. For applications where less precision is required, lower-cost laser diodes can also be used with the OPA optical tweezers; however, if temperature stabilization circuitry is not included with the laser, wavelength stability will begin to have a noticeable effect on the stiffness and maximum force of the trap.

Results

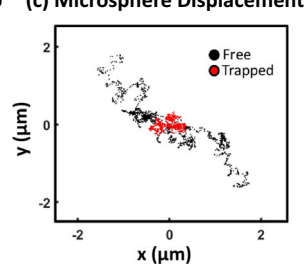
Using this focusing integrated OPA system, we now demonstrate optical trapping and tweezing with an integrated OPA for the first time, increasing the standoff distance of integrated optical tweezers by over two orders of magnitude compared to prior demonstrations⁹⁻¹⁵. Specifically, we calibrate the trap force of the system and demonstrate both optical trapping and tweezing of polystyrene microspheres using the system. We then use the OPA system to perform, for the first time, cell experiments with single-beam integrated optical tweezers. Specifically, we show controlled deformation of mouse lymphoblast cells, a biologically-relevant technique that can be used to determine the elastic moduli of cells for both fundamental research and elucidation of disease mechanisms.

Optical trapping of polystyrene microspheres with integrated OPA tweezers

First, we use the OPA system to demonstrate optical trapping of polystyrene microspheres. These experiments demonstrate the system's utility in standard biophysics experiments, which commonly use

(a) Characterization Setup

(b) Experimental Trapping Demo (c) Microsphere Displacement



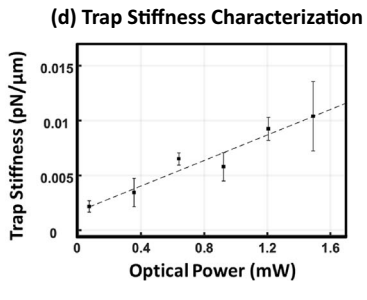


Fig. 3 | Optical trapping of polystyrene microspheres with integrated OPA tweezers. a Photograph of the experimental setup, showing the input optical fiber, OPA chip, sample stage holding a well filled with microsphere solution, and imaging objective. **b** Micrograph of the microspheres in the sample well with superimposed tracks showing their motion over time (red lines); the motion of the microsphere located at the focal spot of the OPA (circled in white) is significantly reduced

compared to its neighbors, indicating successful trapping. c Two-dimensional position over time of a microsphere before (black) and after (red) the trap is turned on; position is normalized to the origin at the start of free and trapped tracks. **d** Measured trap stiffness versus optical power in the trap focal spot for polystyrene microsphere trapping; error bars are found by calculating the standard error of the dataset.

polystyrene microspheres as handles for biological molecules of interest^{6,25}.

The setup used to characterize our integrated OPA-based optical trap is shown in Fig. 3a. The optical trap chip is mounted on a chuck, with a sample stage that supports either coverslips or small cell culture dishes mounted on a positioning system above the chip. Light is routed from a tunable benchtop laser source via an SMF-28e lensed fiber and is edge coupled to the system with 190 µW of power supplied at the input of the chip. The setup is visualized using either a 20X or a 100X Mitutoyo objective, and split into both visible and IR imaging paths using a dichroic mirror and relay lens.

To create a well for the solution of polystyrene microspheres, two coverslips are separated by double-sided tape, creating a chamber with a thickness of 375 µm, into which a 5.5% v/v solution of polystyrene microspheres suspended in deionized water is pipetted. Specifically, we use microspheres with a diameter of 10 µm and a 0.09-um size distribution, as they have a similar size to human and mouse cells, such as lymphoblasts²⁶. The microspheres come to rest slightly above, but not in contact with, the coverslip surface. The well containing the microsphere solution is then clamped into the sample stage above the chip. Using the positioning system on the sample stage, a target sphere is moved into the focal spot of the trap. Once the sphere moves stably into the center of the trap, its motion is recorded using a visible camera for 75 s. In order to verify that the motion of the sphere of interest is indeed reduced specifically due to the optical trap, the laser is then turned off and the sphere's motion is recorded for an additional 75s while freely moving.

Using the TrackMate plugin for ImageJ²⁷, we track the motion of a group of microspheres during this experiment, of which the middle target sphere is trapped and the other two are free to move, as shown in Fig. 3b. The superimposed red lines show the positions of these three spheres tracked over time. The two freely-moving spheres exhibit movement largely under the influence of Brownian motion, with the additional influence of a directional fluid flow caused by evaporation of the sample from one of its edges. In contrast, one can observe significantly reduced motion in the target trapped sphere. As shown in Fig. 3c, when the laser is off, the target sphere of interest exhibits significant displacement; in contrast, when the laser is on and the sphere is trapped, its motion is severely restricted, indicating that it has successfully been caught in a potential energy well created by the optical trap.

This is the first demonstration of an integrated optical trap able to operate at a millimeter-scale standoff distance, allowing for interaction with samples in standard glass coverslips, eliminating the need for complex microfluidics packaging, and enabling compatibility with a greater variety of samples.

Trap force calibration with polystyrene microspheres

Second, we use the polystyrene microspheres and setup introduced in the preceding section to calibrate the trap force of the integrated OPAbased optical trap.

Using the equipartition theorem and the mean squared displacement $\langle x^2 \rangle$ of a trapped particle in two dimensions, we can calibrate the trap's stiffness using the following equation²⁸,

$$U = k_B T = \frac{1}{2} k(P) \langle x^2 \rangle \tag{1}$$

where T is the sample temperature and k_B is the Boltzmann constant. The trap stiffness should increase linearly as a function of input power²⁹.

To demonstrate this, we measure the mean squared displacement of spheres in the optical trap, tracking their movement using Track-Mate over a 75-second time window as described in the preceding section. We perform N=4 repeated measurements over a range of input powers to calibrate trap stiffness, with each experiment using a fresh sample. Figure 3d shows this measured trap stiffness as a function of optical power in the trap focal spot, with error bars calculated as the standard error of the set of measurements. The results follow the expected linear trend. The linear stiffness behavior of this trap with power demonstrates that it can be calibrated and utilized for force measurement with the same facile equipartition method commonly used with its more mature, standard bulk-optic counterparts^{6,29}.

Note that, at zero optical power, we expect the trap stiffness to reach zero and for our linear fit to therefore pass through the origin. The small nonzero trap stiffness at zero optical power that can be extrapolated from our trendline is an expected characteristic of trap stiffness measured using the equipartition theorem with a finite time window^{30,31} (since zero stiffness corresponds to infinite positional variance for these measurements, an infinite time window is required to capture a stiffness of exactly zero; resultingly, any finite capture window will result in a nonzero reported stiffness, even for zero optical power). This overestimation effect is most significant near zero optical power³¹. In contrast, at higher optical powers, we observe that the trap stiffness generally converges rapidly as a function of capture time, and, therefore, the impact of the finite time window on the trap-stiffness estimation in Fig. 3d is less significant. In the future, with the use of a high-speed camera, power-spectral-density analysis could instead be used to even more accurately characterize the trap stiffness at lower optical powers¹¹.

Optical tweezing of polystyrene microspheres with integrated **OPA** tweezers

Third, we use the OPA system to demonstrate optical tweezing of polystyrene microspheres.

While stationary trapping is useful for many experiments, the ability to manipulate an object in a trap significantly extends the functionality and usability of optical traps. This functionality is known as optical tweezing, and is a capability absent in many integrated optical trapping demonstrations to date^{12,13}.

To enable this tweezing functionality, we leverage the non-mechanical spot steering capability of our OPA system to transform the system from a static optical trap to dynamic optical tweezers. As discussed above, we can vary the wavelength of the laser input into the focusing OPA system to non-mechanically steer the location of the spot emitted out of the OPA—i.e. set the trap position—with micron precision over a range of over a millimeter along the antenna dimension (Fig. 2f). The focal spot remains largely in the sample plane over a steering range of tens of microns.

Using this wavelength-control scheme and an optical power of 1.58 mW in the trap focal spot, we varied the trap position in the antenna dimension, with the polystyrene microsphere following its motion. To confirm that the microsphere was moving successfully due to repositioning of the focal spot and not due to any residual fluid velocity in the sample chamber, we non-mechanically steered the trap back and forth several times and observed the resulting position of the microsphere (Fig. 4b), confirming successful tweezing. Next, we showed repeated tweezing of the microsphere in a sine-wave pattern with two different frequencies, to demonstrate that the microsphere of interest can be steered in arbitrary patterns in one dimension. Specifically, we varied the input laser wavelength as a function of time using two sinusoidal patterns with wavelength ranges of ±1nm, at rates of both 0.059 and 0.048 cycles/min. The resulting position of the trapped microsphere was recorded and processed using TrackMate. The microsphere position (solid line) closely followed the focal spot position (dashed line) for both patterns, demonstrating manipulation with submicron precision over a range of tens of microns (Fig. 4c).

To further confirm the functionality of the system, we then used our integrated optical tweezers to demonstrate tweezing at four different speeds. Specifically, we varied the input wavelength linearly as a function of time for four different wavelength sweep settings (5 pm/s, 6.25 pm/s, 8.33 pm/s, and 12.5 pm/s), resulting in focal spot travel speeds of approximately 60 nm/s, 75 nm/s, 100 nm/s, and 150 nm/s, respectively. Figure 4d shows the resulting measured positions of the trap focal spot and of the target microsphere as a function of time as dashed and solid lines, respectively, for each of the four sweep settings. The microsphere is able to successfully follow the motion of the

focal spot up to a wavelength sweep setting of around 12.5 pm/s (corresponding to a focal spot speed of approximately 150 nm/s), at which point the microsphere begins to fall out of the trap. At this point, the drag force on the particle through the water overcomes the force exerted by the trap, and the sphere lags behind the trap maximum until it falls out of the trap. Note that slightly higher manipulation speeds were attainable in the upwards direction than in the downwards direction, which can be attributed to the asymmetry in the focal spot pattern (Fig. 2e); this asymmetry is common to antennas with constant perturbations and can be improved upon by varying the perturbation strength along the length of the antenna²⁰⁻²².

Although these experiments were performed with a benchtop tunable laser in order to accurately characterize the system and maximize repeatability, this functionality and wavelength tuning range could be readily achieved by powering the system using an inexpensive laser diode with thermal tuning or even an on-chip integrated tunable laser on the same photonic chip^{32,33}.

Optical-tweezers-induced stretching of biological cells with integrated OPA tweezers

Finally, we use the OPA system to perform, for the first time, cell experiments with single-beam integrated optical tweezers, showing controlled deformation of mouse lymphoblast cells.

While the manipulation of polystyrene microspheres is relevant to a wide range of biophysical experiments using optical tweezers, the extension of trapping to cells has yielded highimpact fundamental and applied research, including technologies such as optical cell sorting and novel cancer diagnostics³⁴⁻³⁶. One challenge for optical trapping of cells is that the magnitude of the gradient force depends on the ratio of refractive indices between the particle of interest and the background media. This ratio is 1.19 for polystyrene in a water solution³⁷ versus only about 1.03-1.05 for cells in a water solution^{38,39} at a wavelength of 1550 nm. Consequently, manipulation of cells usually requires higher optical trapping powers. In addition, cells are easily contaminated, and their placement on unique substrates, such as silicon-photonics chips, can stress them and affect the behavior under study^{40,41}. To date, cell manipulation with a single-beam integrated optical trap has yet to be demonstrated. Importantly, the inability to use prior integrated optical tweezers with sterile coverslips or cell culture wells due to their short focal heights, which are too short to penetrate into these sample chambers, has

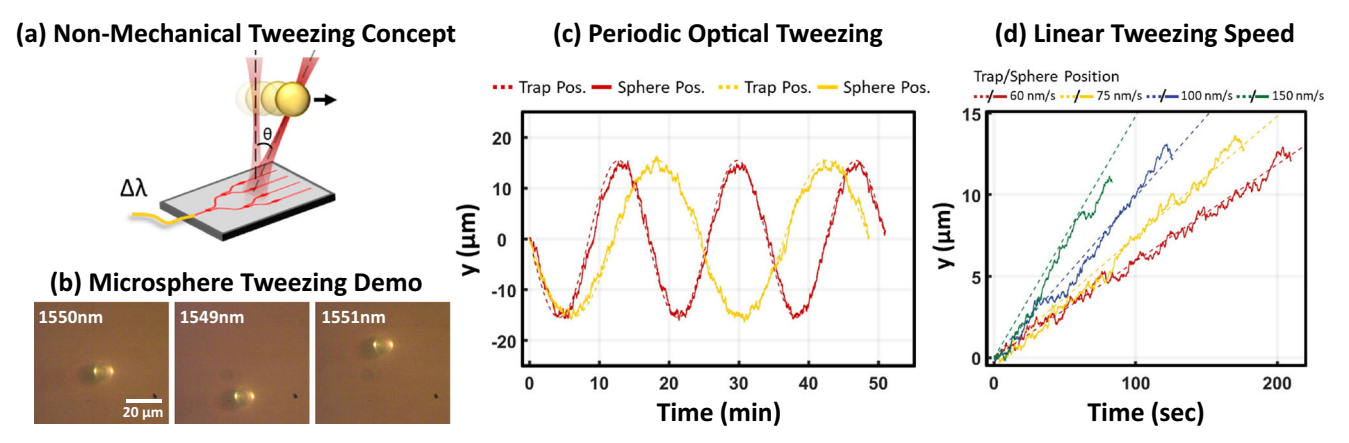


Fig. 4 | **Optical tweezing of polystyrene microspheres with integrated OPA tweezers. a** Conceptual diagram depicting microsphere tweezing using an OPA by varying the input laser wavelength. **b** Micrographs showing the position of a microsphere for input wavelengths of 1550 nm (left), 1549 nm (center), and 1551 nm (right); the position varies with input wavelength, confirming successful tweezing of the microsphere using the OPA tweezers. **c** Position of

the spot formed by the optical trap (dashed line) and position of the optically tweezed microsphere (solid line) vs time for two different sinusoidal wavelength control signals, demonstrating consistent tweezing over arbitrary 1D patterns. **d** Position of the spot formed by the optical trap (dashed line) and position of the optically tweezed microsphere (solid line) vs time for four different linear wavelength sweep settings.

made such demonstrations difficult to realize until now. Herein, we report the first cell experiments with single-beam integrated optical tweezers, performing optical stretching on TIB-49 mouse lymphoblast cells as one example of a proof-of-concept experiment. (Cell deformation using optical tweezers has emerged as a powerful technique for determining the elastic moduli of cells, and has been used in both fundamental research into the mechanical properties of cells and applied studies to investigate disease mechanisms^{36,42-44}, for example diabetic retinopathy⁴⁵.)

In this experiment, we cultured TIB-49 mouse lymphoblast cells in RPMI-1640 media with 10% Fetal Bovine Serum and 1% 10,000 U/mL Penicillin-Streptomycin. We incubated the cells at 37 °C in a humidified 5% CO₂ incubator, removed the cells from the incubator one day after passage, and pipetted them into a 300-µm-thick chamber formed from two coverslips separated by double-sided tape. We positioned a cell in the optical trap with an optical power of 1.74 mW in the trap focal spot (Fig. 5a) and then steered the trap in the -y direction in the focal plane by reducing the input laser wavelength. We recorded the cell using a visible camera and observed that the bottom edge of the cell was attracted to the new trap position (Fig. 5b), leading to an increase in the cell aspect ratio of over 25% along the long axis of the cell. The cell has some inherent attraction to the surface of the coverslip, and, as a result, the edge of the cell outside of the trap remains in its position and cell deformation as opposed to movement of the entire cell is observed. Upon turning off the laser, the cell relaxed to its prior unstretched state (Fig. 5c). As a control reference, when the optical trap input laser is powered off, no noticeable deformation of cells was seen over a period of several minutes, indicating that the observed deformation with wavelength tuning is indeed due to the influence of the optical trap (Fig. 5d). Note that we observed that samples in which cells showed significant stress granules would not deform under the influence of optical tweezers; this highlights the sensitivity of the mechanical properties of cells to their environment, and makes a compelling case for the need for greater experimental flexibility afforded by the millimeter-scale standoff distance of our OPA-based optical tweezers.

Discussion

In summary, this work presents optical trapping and tweezing using an integrated OPA for the first time, increasing the standoff distance of integrated optical tweezers by over two orders of magnitude larger than prior demonstrations, significantly expanding their utility. We use a focusing integrated OPA to emit a tightly focused beam out of the chip and demonstrate successful trapping of polystyrene microspheres 5 mm above the surface of the chip, with the sphere's motion significantly reduced due to the force of the trap. We next calibrate this

optical trap system using the equipartition method, a common calibration method for bulk optical tweezers²⁸, demonstrating consistent trap stiffness that scales linearly with power. We then non-mechanically steer the focal spot by varying the input laser wavelength to transform the system from a static optical trap to dynamic optical tweezers and demonstrate tweezing of polystyrene microspheres in one-dimensional patterns with high fidelity and submicron precision. Finally, we use these OPA tweezers to show controlled deformation of mouse lymphoblast cells (a biologically-relevant technique that can be used to analyze mechanical properties of cells for both fundamental research and applied studies to investigate disease mechanisms^{42–45}), a promising proof-of-concept demonstration that represents, to the best of our knowledge, the first cell experiments using single-beam integrated optical tweezers.

In the future, given the natural scalability and design flexibility of the CMOS-compatible fabrication platform used to produce these OPA tweezers, there are a number of natural opportunities to further evolve the system to both improve its performance and enable new functionality. First, the integrated OPA could be scaled to a larger aperture size²³ and the perturbation strength of the antennas in the OPA could be apodized²⁰⁻²², which would decrease the diameter and increase the symmetry of the focal spot²³, improvements which would further improve the trap stiffness and uniformity. Second, silicon nitride could be used as the waveguiding material for the integrated OPA to improve the optical power handling capability of the waveguides and enable significantly more powerful optical tweezers that operate in a different force regime (standard silicon waveguides have limited power handling capability due to two-photon absorption⁴⁶). Third, novel focusing OPA architectures that incorporate electro-optic or thermo-optic modulators could be developed that enable non-mechanical two- or three-dimensional steering of the focal spot and do not require a tunable laser source²³. These future OPA architectures could also be designed to encode advanced holographic emission patterns of interest⁴⁷, such as closely-spaced arrays of traps for high-throughput trapping applications^{34,48}. Fourth, by leveraging the small form factor and high integration density enabled by CMOS processing, multiple integrated OPA tweezers could be integrated together in a massively parallel configuration, enabling applications in high-throughput cell sorting and diagnostic tools. Fifth, by taking advantage of the advanced functionality enabled by CMOS processing, OPA tweezers could be monolithically integrated with germanium detectors, a standard offering in existing silicon-photonics process design kits¹⁹, to create optical tweezers that simultaneously measure the position of the trapped object using the deflection of the trapping beam. Sixth, using the flexible-wafer silicon-photonics fabrication process recently developed by our group⁴⁹, this OPA tweezers system could even be

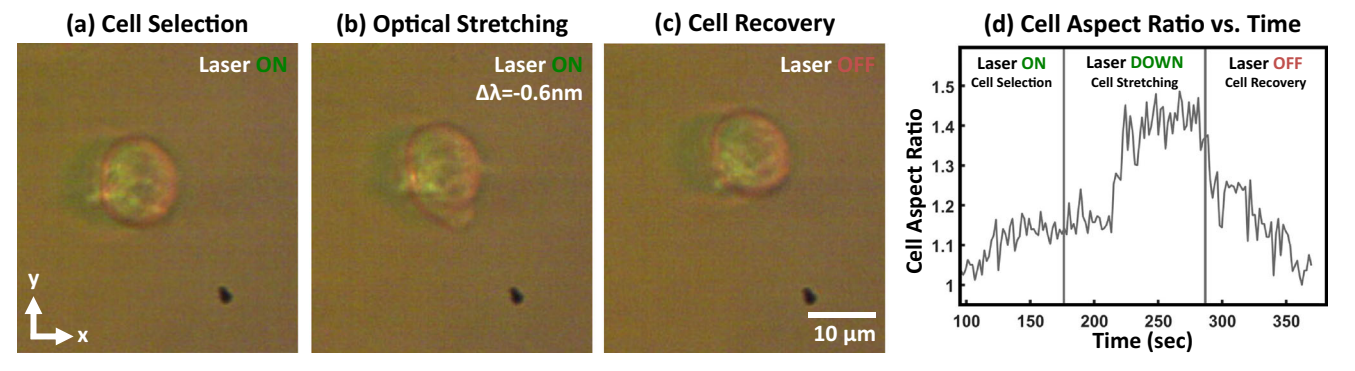


Fig. 5 | **Optical manipulation of biological cells with integrated OPA tweezers. a** Micrograph showing a TIB-49 mouse lymphoblast cell trapped in the focus of the optical trap. **b** The wavelength of the input laser is reduced by 0.6 nm, steering the trap focus in the -y direction below the cell; the cell is stretched

downward by the movement of the trap. **c** Upon turning off the laser, the cell regains its original unstretched dimensions. **d** The cell's aspect ratio is tracked versus time, demonstrating large deformation in response to repositioning of the trap location.

extended to a wearable diagnostic, contributing to the emerging field of in-vivo optical trapping⁷.

Overall, this work introduces a new modality for integrated optical tweezers, presenting a fundamentally different approach to optical tweezers based on integrated OPAs that enables significantly larger standoff distances and arbitrary active tweezing functionality. The large focal heights enabled by this approach allow for manipulation of samples in simple coverslips and sample chambers standard to biological experiments (and even the potential to probe into the body for future in-vivo applications⁷), eliminating the need for complex microfluidics packaging that has been a necessary component of prior integrated optical tweezers demonstrations. This OPA-based approach offers the advantages in cost, footprint, complexity, and mass producibility of integrated tweezers, while providing much of the functionality of bulkoptical systems. It thus represents a significant improvement in the future utility and compatibility of integrated optical tweezers for biological research and has the potential to open the door to a wide variety of experiments that have not been previously possible with prior implementations of integrated tweezers, spanning biophysics research with microsphere-conjugated molecules, single-cell experimentation and sorting, and emerging in-vivo trapping research.

Methods

Integrated-optical-phased-array chip fabrication

The integrated-optical-phased-array system was fabricated in a CMOS-compatible 300-mm-diameter wafer-scale silicon-photonics process at the State University of New York Polytechnic Institute's (SUNY Poly) Albany NanoTech Complex. The process utilizes 300-mm-diameter silicon-on-insulator (SOI) wafers with a 2- μ m-thick buried oxide and a standard 220-nm-thick silicon waveguiding layer patterned using 193-nm immersion lithography. Details are provided in 23 .

Experimental characterization setup

The integrated OPA-based optical tweezers were characterized using an optical imaging system consisting of a microscope objective (Mitutoyo, either 20X/0.4NA or 100X/0.5NA), and separate IR and visible imaging paths. The microscope objective is connected to a dichroic mirror, which routes light into a visible camera and, via a relay lens, to an IR camera. This system is mounted on an optical breadboard with three axes of movement. The tweezers chip is mounted on a chuck. Light is routed from an Agilent 81600B tunable benchtop laser source through an Amonics erbium-doped fiber amplifier (AEDFA-C_20I-B) to an SMF-28e lensed fiber that is edge coupled to the silicon-photonics chip. A sample stage that supports both coverslips and small cell culture dishes is mounted on a NanoMax positioning system above the chip.

Focal-spot and beam-steering characterization

Characterization of the focusing beam formation and beam-steering functionality of the integrated optical tweezers was achieved by recording images of the light emitted out of the chip using a high-resolution IR camera (SUI Goodrich SU640KTS-1.7RT). The height of the optical imaging system was then set such that images were taken at the focal plane of the OPA, with the focal plane location determined by scanning the system to the height above the chip where the focusing beam generates the minimum focal spot size. Focal plane images were then recorded over a range of input wavelengths to characterize the wavelength-induced non-mechanical beam-steering functionality. The locations of the intensity maxima were determined in MATLAB, and the resulting spatial offset of the beam in the steering direction was plotted as a function of the input wavelength. More details are provided in²³.

Glass coverslip chamber assembly

Chambers either 300 µm or 375 µm in height were formed between two #1 coverslips (VWR Microscope Cover Glasses, 16004-308) separated

by several pieces of double-sided tape of thickness 75 μ m according to the target chamber height. The chamber was mounted on a larger #1 coverslip for compatibility with the sample stage.

Polystyrene microsphere preparation

Polystyrene microspheres (Duke Standards 4210A, 0.9% CV) were suspended in deionized water as a 5.5% v/v solution.

Data acquisition and processing for microsphere experiments

Microsphere movements were recorded using an iDS UEye 1480-LE-C-HQ visible camera, recording with 640×480 resolution at 13.5 FPS, using dual-arm fiber optic illumination. The recorded video was loaded into the ImageJ plugin TrackMate. Spots marking the microspheres' position in a given frame were found with a Laplace of Gaussian detection algorithm using the reflections off the sides of the spheres, which present as two bright dots on the lateral edges of each bead. Tracks were exported and processed in Python.

Cell culture

TIB-49 mammalian cells were acquired from ATCC. Cells were maintained in a T-25 flask (ThermoFisher Scientific) containing RPMI-1640 Medium (ThermoFisher Scientific) with 10% Fetal Bovine Serum (ThermoFisher Scientific) and $1\%\,10,000\,U/mL$ Penicillin-Streptomycin (ThermoFisher Scientific). Cells were stored at 37 °C in a humidified 5% CO_2 incubator and were passaged one day prior to experimentation. Following harvesting, cells were washed through the use of a centrifuge and resuspended into a fresh media solution.

Cell tweezing and processing

Cells were removed from the incubator and pipetted into a chamber with a thickness of $300\,\mu m$ formed between two #1 coverslips. Cells were maneuvered into the focal spot emitted out of the integrated optical tweezers, which were then non-mechanically steered beyond the cell boundary. Cell deformation was recorded using a visible camera. The optical tweezers were then turned off to record the cell's behavior in the absence of the force of the optical trap.

Reporting summary

Further information on research design is available in the Nature Portfolio Reporting Summary linked to this article.

Data availability

Data is available upon request.

References

- Ashkin, A. Acceleration and trapping of particles by radiation pressure. Phys. Rev. Lett. 24, 156–159 (1970).
- Ashkin, A. & Dziedzic, J. M. Optical trapping and manipulation of viruses and bacteria. Science 235, 1517–1520 (1987).
- Marago, O. M., Jones, P. H., Gucciardi, P. G., Volpe, G. & Ferrari, A. C.
 Optical trapping and manipulation of nanostructures. *Nat. Nanotechnol.* 8, 807–819 (2013).
- Pang, Y., Song, H., Kim, J. H., Hou, X. & Cheng, W. Optical trapping of individual human immunodeficiency viruses in culture fluid reveals heterogeneity with single-molecule resolution. *Nat. Nano*technol. 9, 624–630 (2014).
- Bouloumis, T. D. & Chormaic, S. N. From far-field to near-field microand nanoparticle optical trapping. Appl. Sci. 10, 1375 (2020).
- Arbore, C. et al. α-catenin switches between a slip and an asymmetric catch bond with F-actin to cooperatively regulate cell junction fluidity. Nat. Commun. 13, 1146 (2022).
- Zhong, M. C., Wei, X. B., Zhou, J. H., Wang, Z. Q. & Li, Y. M. Trapping red blood cells in living animals using optical tweezers. *Nat. Commun.* 4, 1768 (2013).

- Sun, Y. Y. et al. Large-scale optical traps on a chip for optical sorting. Appl. Phys. Lett. 90, 031107 (2007).
- Soltani, M. et al. Nanophotonic trapping for precise manipulation of biomolecular arrays. Nat. Nanotechnol. 9, 448–452 (2014).
- 10. Renaut, C. et al. On chip shapeable optical tweezers. Sci. Rep. 3, 2290 (2013).
- Ye, F., Inman, J. T., Hong, Y., Hall, P. M. & Wang, M. D. Resonator nanophotonic standing-wave array trap for single-molecule manipulation and measurement. *Nat. Commun.* 13, 77 (2022).
- 12. Yu, S. et al. On-chip optical tweezers based on freeform optics. Optica **8**, 409–414 (2021).
- 13. Juan, M. L., Righini, M. & Quidant, R. Plasmon nano-optical tweezers. *Nat. Photon.* **5**, 349–356 (2011).
- Yang, A. H. et al. Optical manipulation of nanoparticles and biomolecules in sub-wavelength slot waveguides. Nature 457, 71–75 (2009).
- Ahluwalia, B. S., McCourt, P., Huser, T. & Helleso, O. G. Optical trapping and propulsion of red blood cells on waveguide surfaces. Opt. Express 18, 21053–21061 (2010).
- Righini, M., Volpe, G., Girard, C., Petrov, D. & Quidant, R. Surface plasmon optical tweezers: tunable optical manipulation in the femtonewton range. *Phys. Rev. Lett.* **100**, 186804 (2008).
- 17. Notaros, J. et al. CMOS-compatible optical phased array powered by a monolithically-integrated erbium laser. *J. Light. Technol.* **37**, 5982 (2019).
- Poulton, C. V. et al. Long-range LiDAR and free-space data communication with high-performance optical phased arrays. *IEEE J. Sel. Top. Quantum Electron.* 25, 1–8 (2019).
- Bhargava, P. et al. Fully integrated coherent LiDAR in 3D-integrated silicon photonics/65nm CMOS. In 2019 Symposium on VLSI Circuits, Kyoto, Japan. C262–C263 (2019).
- Kim, T. et al. A single-chip optical phased array in a wafer-scale silicon photonics/CMOS 3D-integration platform. *IEEE J. Solid-State Circuits* 54, 3061–3074 (2019).
- Heck, M. J. R. Highly integrated optical phased arrays: photonic integrated circuits for optical beam shaping and beam steering. *Nanophotonics* 6, 93–107 (2017).
- Raval, M., Poulton, C. V. & Watts, M. R. Unidirectional waveguide grating antennas with uniform emission for optical phased arrays. Opt. Lett. 42, 2563–2566 (2017).
- 23. Notaros, J., Poulton, C. V., Raval, M. & Watts, M. R. Near-field-focusing integrated optical phased arrays. *J. Light. Technol.* **36**, 5912–5920 (2018).
- 24. Zhang, Y. et al. A compact and low loss Y-junction for submicron silicon waveguide. *Opt. Express* **21**, 1310–1316 (2013).
- Wang, M. D., Yin, H., Landick, R., Gelles, J. & Block, S. M. Stretching DNA with optical tweezers. *Biophys. J.* 72, 1335–1346 (1997).
- Monroe, J. G. & Cambier, J. C. Sorting of B lymphoblasts based upon cell diameter provides cell populations enriched in different stages of cell cycle. J. Immunol. Methods 63, 45–56 (1983).
- 27. Tinevez, J. Y. et al. TrackMate: an open and extensible platform for single-particle tracking. *Methods* **115**, 80–90 (2017).
- 28. Pesce, G. et al. A step-by-step guide to the realisation of advanced optical tweezers. *J. Opt. Soc. Am. B* **32**, 84–98 (2015).
- 29. Felgner, H., Muller, O. & Schliwa, M. Calibration of light forces in optical tweezers. *Appl. Opt.* **34**, 977–982 (1995).
- 30. Perez-Garcia, L. et al. Optimal calibration of optical tweezers with arbitrary integration time and sampling frequencies: a general framework. *Biomed. Opt. Express* **14**, 6442–6469 (2023).
- 31. Sarshar, M., Wong, W. T. & Anvari, B. Comparative study of methods to calibrate the stiffness of a single-beam gradient-force optical tweezers over various laser trapping powers. *J. Biomed. Opt.* **19**, 115001 (2014).
- Li, N. et al. Monolithically integrated erbium-doped tunable laser on a CMOS-compatible silicon photonics platform. Opt. Express 26, 16200–16211 (2018).

- Morton, P. A. et al. Integrated coherent tunable laser (ICTL) with ultra-wideband wavelength tuning and sub-100 Hz lorentzian linewidth. APL Photon 40, 1802–1809 (2022).
- 34. Schaal, F. et al. Marker-free cell discrimination by holographic optical tweezers. *J. Eur. Opt. Soc.* **4**, 09028 (2009).
- 35. LaFratta, C. N. Optical tweezers for medical diagnostics. *Anal. Bioanal. Chem.* **405**, 5671–5677 (2013).
- 36. Guck, J. et al. Optical deformability as an inherent cell marker for testing malignant transformation and metastatic competence. *Biophys. J.* **88**, 3689–3698 (2005).
- Sultanova, N. G., Kasarova, S. & Nikolov, I. Dispersion properties of optical polymers. Acta Phys. Pol. 116, 585–587 (2009).
- Bohannon, K. P., Holz, R. W. & Axelrod, D. Refractive index imaging of cells with variable-angle near-total internal reflection (TIR) microscopy. *Microsc. Microanal.* 23, 978–988 (2017).
- Curl, C. L. et al. Refractive index measurement in viable cells using quantitative phase-amplitude microscopy and confocal microscopy. Cytom. A 65, 88–92 (2005).
- Roman, G. T. et al. Single-cell manipulation and analysis using microfluidic devices. *Anal. Bioanal. Chem.* 387, 9–12 (2007).
- 41. Li, S., Huang, N. F. & Hsu, S. Mechanotransduction in endothelial cell migration. *J. Cell Biochem.* **96**, 1110–1126 (2005).
- 42. Mestas, J. & Hughes, C. C. W. Of mice and not men: differences between mouse and human immunology. *J. Immunol.* **172**, 2731–2738 (2004).
- 43. Huang, L., Liang, F., Feng, Y., Zhao, P. & Wang, W. On-chip integrated optical stretching and electrorotation enabling single-cell biophysical analysis. *Microsyst. Nanoeng.* **6**, 57 (2020).
- Rancourt-Grenier, S. et al. Dynamic deformation of red blood cell in dual-trap optical tweezers. Opt. Express 18, 10462–10472 (2010).
- Agrawal, R. et al. Assessment of red blood cell deformability in type
 diabetes mellitus and diabetic retinopathy by dual optical tweezers stretching technique. Sci. Rep. 6, 15873 (2016).
- 46. Zhang, Y. et al. Non-degenerate two-photon absorption in silicon waveguides: analytical and experimental study. *Opt. Express* **23**, 17101–17110 (2015).
- 47. Notaros, J. et al. Integrated-phased-array-based visible-light neareye holographic projector. In *Conference on Lasers and Electro-Optics (CLEO)* (OSA, 2019).
- 48. Cai, Y. et al. Rapid tilted-plane Gerchberg-Saxton algorithm for holographic optical tweezers. *Opt. Express* **28**, 12729–12739 (2020).
- 49. Notaros, M. et al. Mechanically-flexible wafer-scale integrated photonics fabrication platform. Sci. Rep. 14, 10623 (2024).

Acknowledgements

This work was supported by the National Science Foundation Faculty Early Career Development (CAREER) Program (Grant No. 2239525), National Science Foundation Graduate Research Fellowship Program (Grant No. 1122374), MIT Frederick (1953) and Barbara Cronin Fellowship, and MIT Rolf G. Locher Endowed Fellowship. The authors thank Jose Roberto Rodriguez for assistance with cell preparation, Andres Garcia Coleto for assistance with cell experiments, and Christopher V. Poulton and Manan Raval for contributions to prior work on the development, design, and experimental demonstration of the focusing OPA system.

Author contributions

T.S., S.C., and M.N. performed the experiments. T.S., S.C., and M.N. performed the data analysis. K.K. and T.S. prepared the cells. J.V. supervised the cell preparation. J.N. supervised the project. All authors contributed to preparing the manuscript.

Competing interests

The authors declare no competing interests.

Additional information

Supplementary information The online version contains supplementary material available at https://doi.org/10.1038/s41467-024-52273-x.

Correspondence and requests for materials should be addressed to Jelena Notaros.

Peer review information *Nature Communications* thanks the anonymous reviewers for their contribution to the peer review of this work. A peer review file is available.

Reprints and permissions information is available at http://www.nature.com/reprints

Publisher's note Springer Nature remains neutral with regard to jurisdictional claims in published maps and institutional affiliations.

Open Access This article is licensed under a Creative Commons Attribution-NonCommercial-NoDerivatives 4.0 International License, which permits any non-commercial use, sharing, distribution and reproduction in any medium or format, as long as you give appropriate credit to the original author(s) and the source, provide a link to the Creative Commons licence, and indicate if you modified the licensed material. You do not have permission under this licence to share adapted material derived from this article or parts of it. The images or other third party material in this article are included in the article's Creative Commons licence, unless indicated otherwise in a credit line to the material. If material is not included in the article's Creative Commons licence and your intended use is not permitted by statutory regulation or exceeds the permitted use, you will need to obtain permission directly from the copyright holder. To view a copy of this licence, visit http://creativecommons.org/licenses/by-nc-nd/4.0/.

© The Author(s) 2024